

# Diffusion of bedload particles in open-channel flows: distribution of travel times and second-order statistics of particle trajectories

Robert J. Bialik<sup>1</sup> · Vladimir I. Nikora<sup>2</sup> ·  
Mikołaj Karpiński<sup>1</sup> · Paweł M. Rowiński<sup>1</sup>

Received: 19 August 2014 / Accepted: 25 May 2015 / Published online: 2 June 2015  
© The Author(s) 2015. This article is published with open access at Springerlink.com

**Abstract** The motion of bedload particles is diffusive and occurs within at least three scale ranges: local, intermediate and global, each of which with a distinctly different diffusion regime. However, these regimes, extensions of the scale ranges and boundaries between them remain to be better defined and quantified. These issues are explored using a Lagrangian model of saltating grains over the uniform fixed bed. The model combines deterministic particle motion dynamics with stochastic characteristics such as probability distributions of step lengths and resting times. Specifically, it is proposed that a memoryless exponential distribution is an appropriate model for the distribution of rest periods while the probability that a particle stops after a current jump follows a binomial distribution, which is a distribution with lack of memory as well. These distributions are incorporated in the deterministic Lagrangian model of saltating grains and extensive numerical simulations are conducted for the identification of the diffusive behavior of particles at different time scales. Based on the simulations and physical considerations, the local, intermediate, and global scale ranges are quantified and the transitions from one range to another are studied for a spectrum of motion parameters. The obtained results demonstrate that two different time scales should be considered for parameterization of diffusive behavior within intermediate and global scale ranges and for defining the local–intermediate and intermediate–global boundaries. The simulations highlight the importance of the distributions of the step lengths and resting times for the identification of the boundaries (or transition intervals) between the scale ranges.

**Keywords** Lagrangian model · Particle diffusion · Saltation · Sediment transport

---

✉ Robert J. Bialik  
rbialik@igf.edu.pl

<sup>1</sup> Institute of Geophysics, Polish Academy of Sciences, Ks. Janusza 64, Warsaw, Poland

<sup>2</sup> School of Engineering, University of Aberdeen, Aberdeen, UK

## 1 Introduction

It has been proposed that the motion of bedload particles is diffusive [6, 19] and consists of at least three ranges of scales: local, intermediate, and global [16, 17]. The local range relates to the distance that the particle travels during a single jump. The intermediate range corresponds to the longer times, involving many jumps while the global range of scales consists of many intermediate ranges (Fig. 1). Based on physical considerations, Nikora et al. [16, 17] suggested that each of these ranges exhibits a different diffusion regime: ballistic diffusion in the local range  $\gamma = 1$ ; normal  $\gamma \approx 0.5$  or anomalous (super-  $\gamma > 0.5$  or sub-  $\gamma < 0.5$ ) diffusion in the intermediate range; and sub-diffusion  $\gamma < 0.5$  in the global range (Fig. 1). The parameter  $\gamma$  is a scaling (diffusion) exponent in  $\overline{X'^2} \propto t^{2\gamma_x}$  and  $\overline{Y'^2} \propto t^{2\gamma_y}$ , where  $[X, Y]$  are the particle coordinates  $X' = X - \overline{X}$ ,  $Y' = Y - \overline{Y}$ , an overbar defines ensemble averaging, and prime defines the deviation from the mean value. The hypothesis of sub-diffusion in the global range has been motivated by observations that in their motion the particles experience periods of prolonged rests.

The experimental information on the diffusion exponents for all three scale ranges remains scarce making a defensible identification of the diffusion regimes difficult. Furthermore, recent studies highlighted that the scaling behavior within a particular scale range as well as the boundaries between the ranges may depend on specific transport conditions or motion modes [5, 10, 14, 18, 22]. For instance, the transition from the intermediate scale range to the global range, expressed in terms of  $tu_*/d$  ( $t$  is time,  $u_*$  is friction velocity,  $d$  is particle diameter) has been found to vary from tens [14, 17] to hundreds [3, 22]. This discrepancy is likely to be a result of using the same dimensionless argument  $tu_*/d$  for all scale ranges while it may be applicable only at shorter times corresponding to the local and intermediate scale ranges where particle dynamics effects are dominant. The quantification of the transition from the intermediate range to the global range may require another scaling that involves information on the resting times, which is

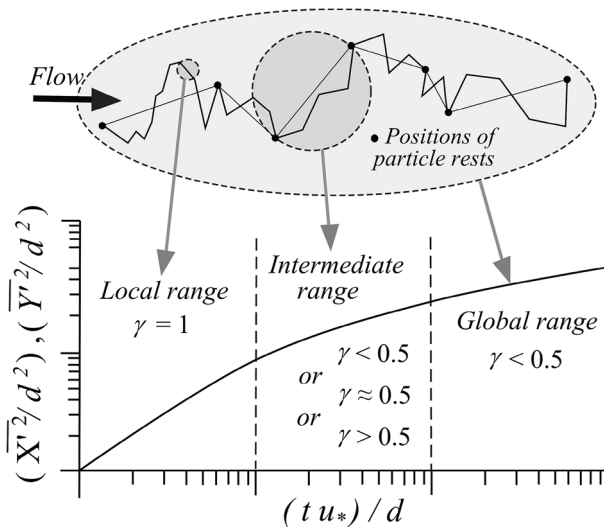


**Fig. 1** Schematic presentation of a conceptual model of a bed particle diffusion, adapted from Nikora et al. [16, 17]

missing in  $tu_*/d$ . To clarify these issues, an approach based on numerical simulations may be useful.

As the diffusion regimes and associated scales reflect statistical properties of the particle motion such as distributions of rest periods and step lengths (e.g., jump lengths at a local scale and/or travel distances between the rests at an intermediate scale), it may be helpful to explore these distributions and involve them into consideration of diffusive properties of moving particles. Available data suggest that particle step lengths at the intermediate scale (i.e., distances between long rests) are likely to follow exponential [7, 8, 13], gamma [12], or two-parameter gamma [11] distributions. In these references, it can also be found that the mean step lengths may vary, depending on travel conditions, from 100 to 150 particle diameters. The information on the empirical distributions of rest periods is less extensive. The available data advocate that this distribution is exponential [7, 8, 11] or follows the power law when the deposited particles are buried by other particles [14, 15, 20]. The information on the step length and resting time distributions can be incorporated in a deterministic Lagrangian model of saltating grains [3], which in turn can provide a basis for extensive numerical simulations for the identification of the diffusive behavior of particles at different time scales.

The objectives of this study therefore include: (1) identification of appropriate probability distributions for step lengths and resting times and expansion of a Lagrangian model of Bialik et al. [3] by combining deterministic particle motion dynamics with these

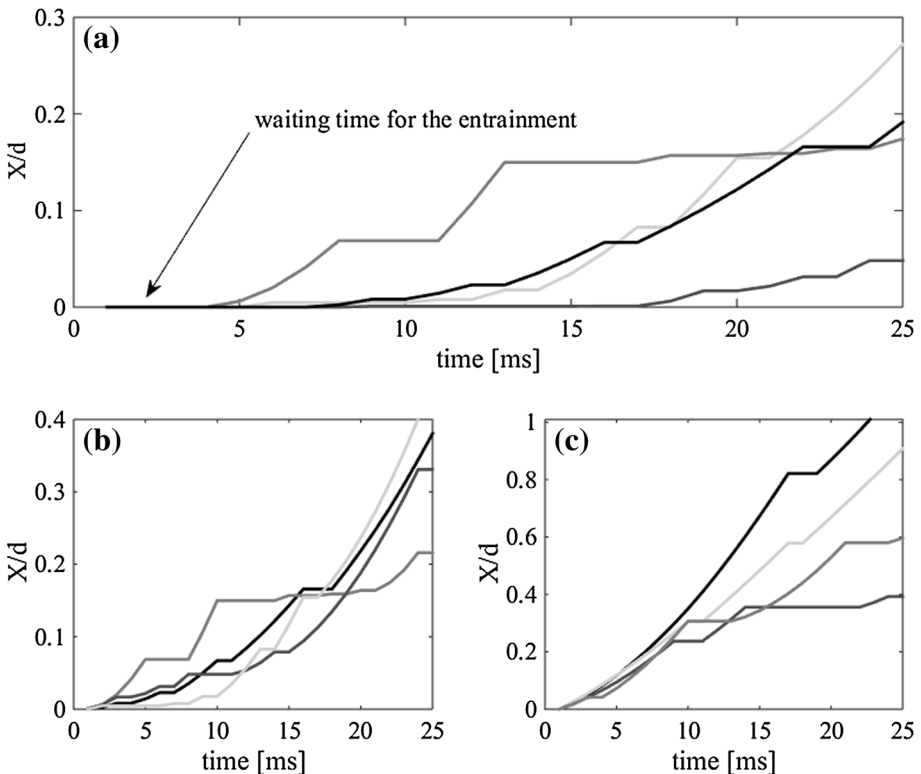


**Fig. 2** Schematic presentation of possible options for selecting starting points for diffusion analysis

distributions; (2) identification of physically-relevant scaling for the time argument in the diffusion relationships suitable for particular ranges of scales; and (3) analysis of the statistical distributions and second-order statistics of particle trajectories, and quantification of diffusion regimes, extensions of the scaling ranges, and the boundaries between them.

Before we proceed to the next section, it should be noted that there are several potential options for selecting starting points for diffusion analysis. In this paper we analyze the diffusive properties of moving particles by superimposing particle trajectories considering instances of particle ‘placement/release’ on the bed as reference points (i.e., including some waiting time before first entrainment, Fig. 2a), rather than instances of direct entrainment (as in [3], Fig. 2b) or randomly selected points of particle-bed contact (as in [16, 17], Fig. 2c). This approach (i.e., Fig. 2a) permits identification of the ‘near-field’ diffusive behavior [1, 3] instead of the pure ballistic diffusion of already saltating particles. In other words, at small diffusive times the ‘near-field scale’ associated with a particle trajectory just after its ‘release’ on the bed is explicitly resolved in our analysis. More details on the effects of diffusion starting points and their influence on the diffusion regimes can be found in [1, 3, 21].

## 2 Deterministic-stochastic Lagrangian model of particle motion and simulation scenarios

A deterministic-stochastic Lagrangian model of particle motion that we propose here is based on a deterministic 3D model of Bialik et al. [3], which is an extension of the earlier 2D model [2]. The deterministic 3D model represents the balance of the fundamental forces acting on moving particles in a fluid flow: drag force  $\mathbf{F}_D$ , lift force  $\mathbf{F}_L$ , virtual mass force  $\mathbf{F}_v$ , and a gravity force  $\mathbf{F}_g$ . The general form of the underpinning equation of motion is:

$$\rho_p \frac{\pi d^3}{6} \frac{d\mathbf{u}_p}{dt} = \mathbf{F}_D + \mathbf{F}_L + \mathbf{F}_v + \mathbf{F}_g, \quad (1)$$

where  $t$  is time,  $\mathbf{u}_p$  denotes the particle velocity vector,  $\rho_p$  stands for the density of particles, and  $d$  is the diameter of saltating particles. In the model, Eq. (1) is supplemented with a trajectory equation, bed-collision sub-model based on the impulse momentum equations, and a Monte-Carlo generator of flow velocity field, initially proposed in [16] and later also used to simulate saltating grains movement in a 2D model [2]. The model equations can easily be solved numerically using the fourth-order Runge–Kutta method and employing the following initial conditions [3, 4]:  $x_p(t_0) = 0$ ,  $y_p(t_0) = 0$ ,  $z_p(t_0) = 0.5d$ ,  $u_p(t_0) = 0$ ,  $v_p(t_0) = 0$  and  $w_p(t_0) = 0$  to analyze the incipient motion of a particle; coordinates  $x_p$ ,  $y_p$ ,  $z_p$  describe particle positions in streamwise, transverse and vertical directions, respectively, and  $u_p$ ,  $v_p$ ,  $w_p$  are particle velocity components in the streamwise, transverse and vertical directions, respectively. More details on this 3D model including the description of the model for generation of flow velocity field, numerical simulation details, and entrainment procedure can be found in [3].

The described model has been extended in this work by adding a stochastic (Monte-Carlo-type) sub-model that generates data on intermediate step lengths and resting times. This sub-model incorporates the following theoretical reasoning. Let us consider a sequence of Bernoulli trials in which success is a particle stop after its current jump while

its further movement is failure. In addition, let us assume that the particle stops (the first success has occurred) after a number of jumps  $T$ . Then  $P(T > k) = q^k$ , where  $q$  is the probability of failure in the current jump, and  $k \in \mathbb{N}_+$  describes the  $k$ th trial. Next, let us consider that no success has occurred during the first  $R$  jumps. In such a situation,  $P(T > k + R | T > R)$  is also equal to  $q^k$  since:

$$P(T > R + k | T > R) = \frac{P(T > R + k, T > R)}{P(T > R)} = \frac{P(T > R + k)}{P(T > R)} = \frac{q^R q^k}{q^R} = q^k \quad (2)$$

and it is independent of the number of preceding  $R$  failures. Equation (2) expresses a property of exponential and geometrical probability distributions and is called memoryless. It should be noted that from a physical point of view the rest periods and step lengths are likely to be unrelated to each other and that the previous history does not influence the probability of a given particle to be eroded, which was first highlighted by Einstein [7, 8]. Thus, the rest period and step length distributions seem most appropriate for describing statistics of the particle motion, particularly for the case of sediment transport over the uniform fixed bed, where the deposited particle cannot be buried by other particles, as is considered in this study. Sediment transport in a bedrock stream may serve as an example of potential occurrence of the studied case.

Let us invoke the following theorem: “The conditional probability that the waiting time terminates at the  $k$ th trial, assuming that it has not terminated before, equals  $p_0$  (the probability at the first trial). We claim that  $p_k = (1 - p_0)^k p_0$ , so that  $T$  has a geometric distribution” [9]. Let us now assume that the mean travel distance (i.e., step length between entrainment and settlement) is equal to  $N$  particle diameters, and that the particle jumps may be properly described by mean jump length  $L_s$ , obtained based on the numerical simulations using the saltation model. Then the unknown probability  $p$  that the particle will stop after its current jump is equal to:

$$p = \frac{L_s}{N} \quad (3)$$

as according to the theorem quoted above the following relation is hold:

$$\begin{aligned} N &= L_s p + 2L_s p(1 - p) + 3L_s p(1 - p)^2 + 4L_s p(1 - p)^3 + \dots \\ &= L_s p \left( 1 + 2(1 - p) + 3(1 - p)^2 + 4(1 - p)^3 + \dots \right) = L_s p \left( \frac{1}{1 - p} \right) = \frac{L_s}{p} \end{aligned} \quad (4)$$

Thus, a binomial distribution with the probability  $p$  of success for each trial may be applied for the simulation. In addition, assuming that the duration of rest periods, which is a random variable  $Z$ , may be described with the exponential distribution, by analogy with Eq. (2) we obtain:

$$P(Z > t + s | Z > t) = P(Z > s). \quad (5)$$

The above probabilistic relations are combined in this study with the 3D deterministic model, described at the beginning of this section, to generate long trajectories of particle motion covering all three ranges of scales (i.e., local, intermediate, and global). The following parameters were used in the simulations presented in the next section: (i) relative size of the moving particles was selected to be  $d/D = 1$  where  $D$  is the size of the static bed particles and  $d = 2$  mm is the size of mobile particles; (ii) the mobility parameter  $K$  (Eq. 6) was selected to be 1.5, which corresponds to the low bed-load transport rate;

(iii) mean rest periods  $\bar{\tau}$  are selected as  $\bar{\tau} = 0, 10 \text{ s}$ , and  $100 \text{ s}$ ; (iv) the entire diffusion (simulation) time  $t = 2 \text{ h}$ ; and (v) the mean travel distance for the cases with mean periods of rest  $\bar{\tau} \neq 0$  was assumed to be  $N = 120d$ . The mobility parameter  $K$  is defined as:

$$K = \frac{1}{\theta_c} \frac{\rho u_*^2}{(\rho_s - \rho)gd}, \tag{6}$$

where  $\theta_c = 0.05$  is the critical value of the dimensionless bed shear stress known as Shields parameter;  $\rho$  and  $\rho_s$  are the water and sediment densities, respectively;  $g$  is gravity acceleration; and  $u_*$  is the friction velocity.

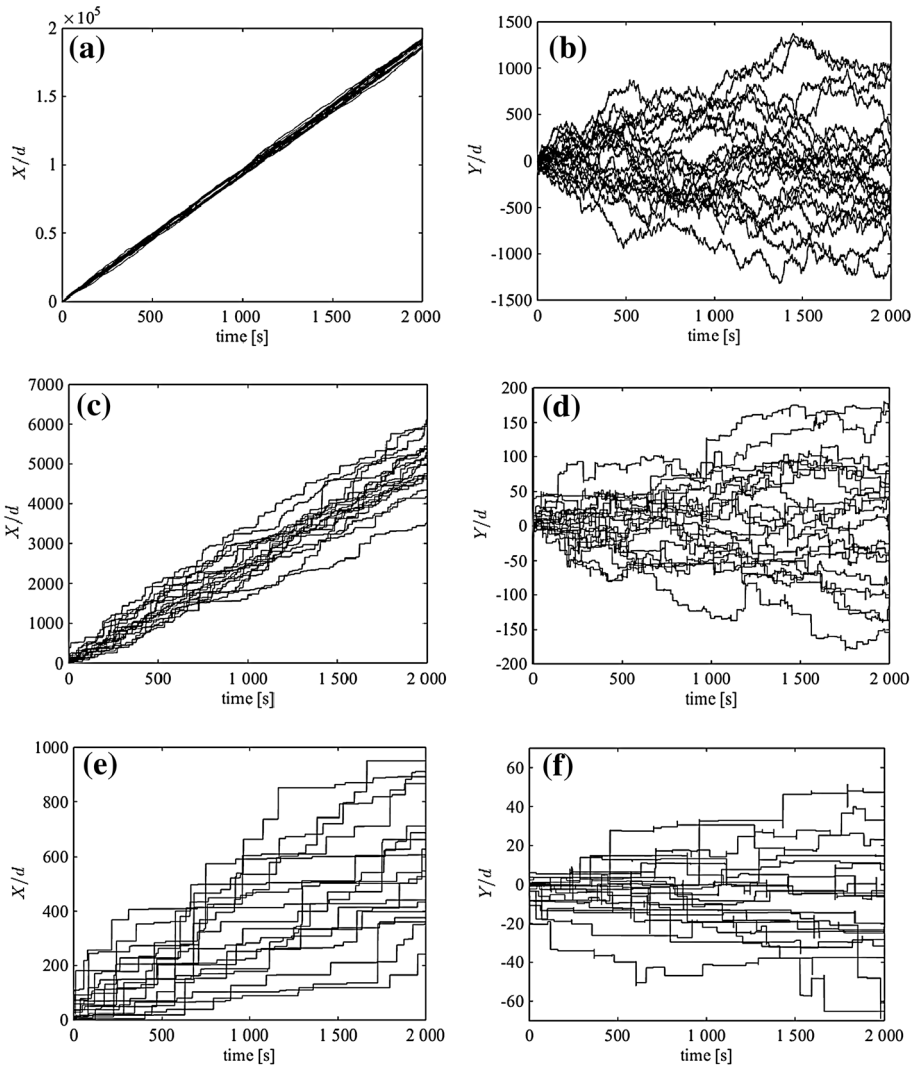


**Fig. 3** Particle trajectories: **a**  $X(t)/d$  and **b**  $Y(t)/d$  for  $\bar{\tau} = 0 \text{ s}$ ; **c**  $X(t)/d$  and **d**  $Y(t)/d$  for  $\tau = 10 \text{ s}$ ; **e**  $X(t)/d$ , and **f**  $Y(t)/d$  for  $\bar{\tau} = 100 \text{ s}$  (for clarity only first 30 min of the simulations are shown)

The particle trajectories including stops and rest periods have been obtained as follows: (i) in the first step, a single jump trajectory between two collisions with the bed is calculated using the 3D model [3]; (ii) second, during each collision with the bed the random number generator, based on the binomial distribution with the probability  $p$ , is used to obtain the logical values of 0 or 1 (if it is 1 then the particle stops after its current jump while if it is 0 then the particle continues motion); (iii) if the particle stops after collision with the bed (the success has occurred), then a duration of a rest period is determined from the exponential distribution with the assumed mean periods of rest  $\bar{\tau}$  from Eq. (5); and (iv) if a failure (the particle has not stopped) occurs, then the next particle jump is calculated and the previous procedure is repeated. The simulation of a sample particle trajectory continued for 2 h and at least 300 trajectories, simulated independently, were obtained and used for calculating the variance of particle positions.

### 3 Scale ranges, their boundaries, and diffusion regimes

Figure 3 shows the examples of temporal changes of the particle locations for three considered cases: (a, b)  $\bar{\tau} = 0$ ; (c, d)  $\bar{\tau} = 10$  s; and (e, f)  $\bar{\tau} = 100$  s. The diffusion behavior can be recognized in all plots. For two cases with non-zero rest periods, the step lengths, particle deposition, and duration of rest periods are clearly identifiable (Fig. 3c–f).

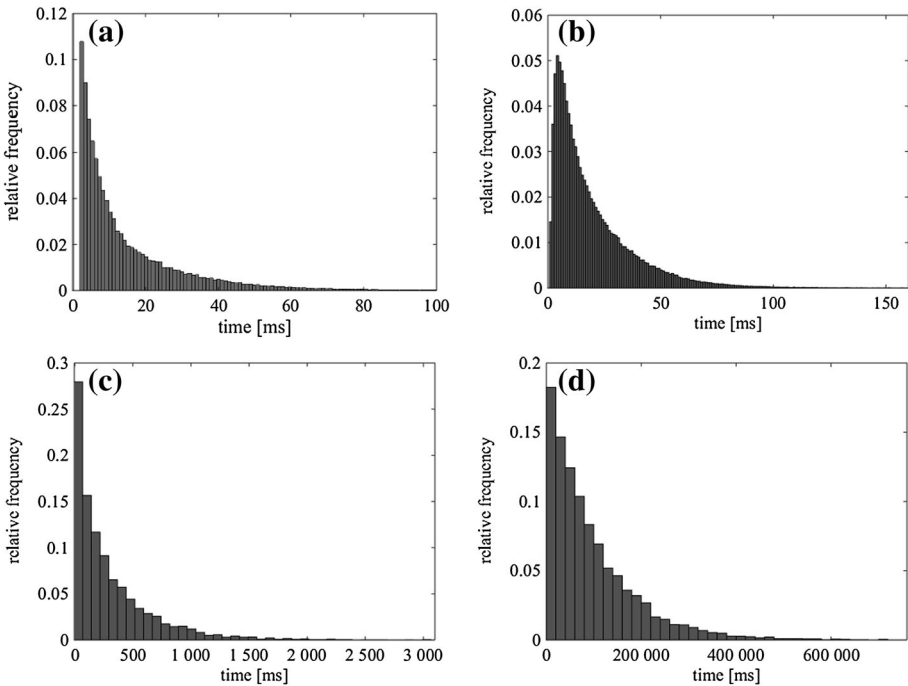


**Fig. 4** Histograms of typical travel times of particle movement for  $\bar{\tau} = 100$  s: **a** acceleration time of a particle after entrainment; **b** single jump time duration (between two consecutive collisions with the bed); **c** travel time between entrainment and stop (disentrainment); and **d** particle travel time between consecutive entrainments

The empirical distributions of specific time periods corresponding to (a) time period of particle acceleration, which is equal to the period of time when the acceleration of a particle after entrainment is greater than zero, (b) durations of individual jumps, (c) travel times between consecutive entrainments and stops (disentrainments), and (d) time periods between consecutive entrainments for the case  $\bar{\tau} = 100$  s are shown in Fig. 4. The distribution of the durations of individual jumps in Fig. 4b resembles a gamma-distribution shape and it quantitatively agrees with the experimental data of Roseberry et al. [18]. Considering the histogram in Fig. 4d it is important to note that the distribution of time periods between consecutive entrainments is a convolution of the exponential-like distribution of the particle travel time from entrainment to stop in Fig. 4c with the assumed exponential distribution of rest periods.

Table 1 summarizes the main statistical parameters for both cases,  $\bar{\tau} = 10$  s and  $\bar{\tau} = 100$  s (in Table 1  $\tau_{95\%}$  defines the 95th quantile). We believe that the data in Table 1 may appear to be instrumental in the identification of specific scale ranges of particle diffusion.

Figure 5 shows the time evolution of the normalized variance of particle positions in the longitudinal and transverse directions, employing the normalized time coordinate  $(tu_*)/d$ . One may observe that for  $\bar{\tau} = 10$  s and  $\bar{\tau} = 100$  s at least five distinct diffusion regimes  $\overline{X^2} \propto t^{2\gamma_X}$  and  $\overline{Y^2} \propto t^{2\gamma_Y}$  with different scaling exponents  $\gamma_X$  and  $\gamma_Y$  can be identified for the  $X$  and  $Y$  coordinates (recall that an overbar defines ensemble averaging while prime defines the deviation from the mean value). For the extreme case of  $\bar{\tau} = 100$  s it is possible to identify the following diffusion regimes in Fig. 5 (95th quantiles of the specific time distributions from Table 1 are used):

- (1) *Local-near-field range* for  $(tu_*)/d < 0.99$  with  $\gamma_X, \gamma_Y \in \langle 2.0, 2.0 \rangle$ ;
- (2) *Local-ballistic range* for  $0.99 < (tu_*)/d < 1.7$  with  $\gamma_X, \gamma_Y \in \langle 1.0, 1.5 \rangle$ ;
- (3) *Intermediate range* for  $1.7 < (tu_*)/d < 22$  with  $\gamma_X, \gamma_Y \in \langle 0.7, 1.0 \rangle$ ;
- (4) *Transition between intermediate and global ranges* for  $22 < (tu_*)/d < 3150$  with  $\gamma_X, \gamma_Y \in \langle 0.12, 0.15 \rangle$  (although the given exponents likely characterize the pseudo-scaling behavior within this range); and
- (5) *Global range* for  $3150 < (tu_*)/d$  with  $\gamma_X, \gamma_Y \in \langle 0.50, 0.50 \rangle$ .

Note that here we subdivided the local range into two subranges: ‘near-field’ subrange influenced by particle acceleration [1] and ballistic sub-range dominated by the particle inertia [16, 17].

At another extreme case without rest periods ( $\bar{\tau} = 0$ ), the global range is not present by definition, while the intermediate range starts at  $(tu_*)/d \sim 30$  and is extended to very

**Table 1** Mean and the 95th quantile values of characteristic times of particle motion for  $\bar{\tau}_{10} = 10$  s and  $\bar{\tau}_{100} = 100$  s

	Time of particle acceleration		Single jump durations		Travel times between entrainments and stops		Travel times between consecutive entrainments	
	(ms)	$tu_*/d$	(ms)	$tu_*/d$	(ms)	$tu_*/d$	(ms)	$tu_*/d$
$\bar{\tau}_{10}$	15	0.32	21	0.44	316	6.64	10,968	230.32
$\tau_{95\%(10)}$	48	1.01	82	1.72	991	20.81	24,268	507.53
$\bar{\tau}_{100}$	15	0.32	21	0.44	310	6.51	96,891	2034.71
$\tau_{95\%(100)}$	47	0.99	81	1.70	1051	22.07	150,051	3151.07



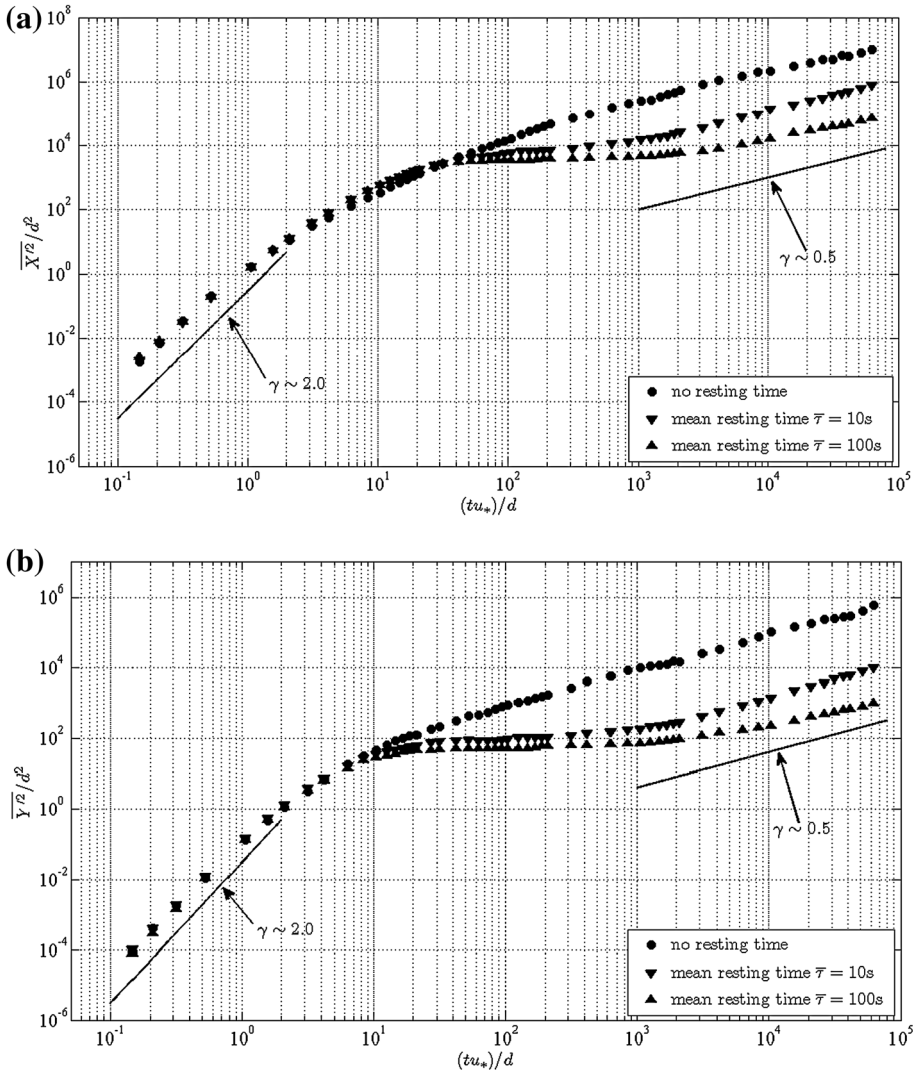


**Fig. 5** Time evolution of the second-order moments of particle positions: **a**  $\overline{X^2}/d^2 = f(tu_*/d)$  and **b**  $\overline{Y^2}/d^2 = f(tu_*/d)$

large diffusion times, with  $\gamma_X \sim 0.50$  and  $\gamma_Y \sim 0.50$ . The difference of these exponents from those shown above for the intermediate range at  $\bar{\tau} = 100$  s can be due to ‘contamination’ of the genuine intermediate range by the effects of the local range at smaller times and by the effects of the global range at larger times. Therefore, the identification of the intermediate range boundaries in Fig. 5 should be treated with caution.

Considering Fig. 5 one may note that at small diffusion times (local and intermediate ranges) the data for different mean resting times  $\bar{\tau}$  collapse around single curves. For the large diffusion times, however, a significant separation of curves occurs pointing to inapplicability of the dimensionless time  $tu_*/d$  for the global range. This could be expected

as moving from the local and intermediate scale ranges to the global range we observe transition from the dominance of the particle dynamics (characterized by  $u_*^2/d$ ) to the dominance of the resting times (characterized by  $\bar{\tau}$ ). Thus, to account for this transition in the dominant factors influencing the particle trajectories, different time normalization for the global range is required. We propose therefore that the time coordinate for the global range should be normalized on  $\bar{\tau}$ . This consideration is strongly supported by the simulation data presented in Fig. 6. In contrast to Fig. 5, the data at large diffusion times in Fig. 6 exhibit a superb collapse on single curves while at small times the data show significant data separation, as one would expect. Figure 6 clearly shows that at large times the variances tend to normal diffusion with  $\overline{X^2} \propto \overline{Y^2} \propto t$ , i.e.,  $\gamma_X = \gamma_Y = 0.5$ .

The success of normalizations  $tu_*/d$  and  $t/\bar{\tau}$  in different ranges of scales highlights that two different mechanisms are responsible for the diffusion of particles in different scale ranges. At small diffusion times related to the local and intermediate ranges the diffusion process is largely controlled by particle dynamics as was suggested by Nikora et al. [17]. At large times associated with the global scale range the diffusion processes are dominated by resting times as supported by numerical simulations in this study.

### 4 Discussion and conclusions

A number of findings in our study, in which a Lagrangian model of saltating grains over the uniform fixed bed was used, contribute to a ‘bigger picture’ of bed particle diffusion. First, the local range in our study exhibits two subranges: (1) ‘near-field’ subrange dominated by the effects of particle acceleration at the beginning of entrainment with  $\gamma_X \sim \gamma_Y \sim 2.0$ , as suggested in [1] and numerically found in [3]; and (2) ballistic subrange due to particle inertia with  $\gamma_X \sim \gamma_Y \sim 1.0$ , as suggested in [16, 17]. This result complements the original conceptual model of Nikora et al. [16, 17] that treated particle diffusion without

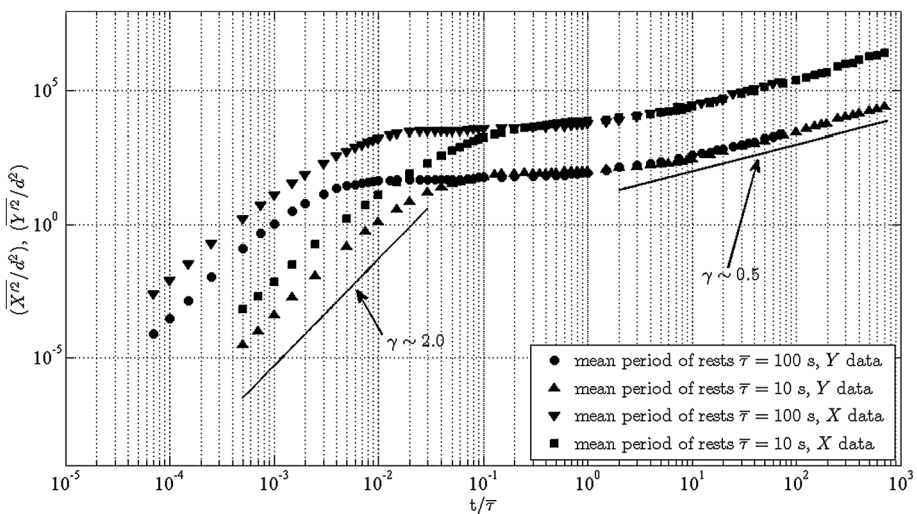


**Fig. 6** Time evolution of the second-order moments of particle positions:  $\overline{X^2}/d = f(t/\bar{\tau})$  and  $\overline{Y^2}/d = f(t/\bar{\tau})$

considering ‘near-field’ acceleration effects. Our simulation results for the local range strongly support analysis of Ballio et al. [1] who found that for the (near-field) local range  $1.0 < \gamma_X < 2.0$  (at least for  $X$  direction) and who explained this result by the initial unsteady phase of particle motion after entrainment. Recently, based on the 3D PIV measurements Witz [21] has also found exponents  $\gamma_X$  for the local range varying from 2.29 to 2.38, which are much greater than for the ballistic diffusion. He explained this difference by the additional streamwise acceleration which allows particles to escape from the bed and move to the saltation mode.

For the intermediate range we found for  $\bar{\tau} = 0$  that  $\gamma_X \sim \gamma_Y \sim 0.5$ , which should also be expected for  $\tau = 10$  s and  $\bar{\tau} = 100$  s. However, Fig. 6 reveals for these cases that the exponents are higher than 0.5, which is likely due to the contamination from the adjacent diffusion ranges. Our findings also suggest that the data of Drake et al. [6], which earlier were interpreted as a global range in [17], are likely to be in a transition from the intermediate range to the global range. The simulation data show that this transition range occurs within  $22 < (tu_*)/d < 3150$ , at least for  $\bar{\tau} = 100$  s and reflects the transition in diffusion mechanisms from particle dynamics dominance to resting times dominance, quantified with  $\bar{\tau}$ . This parameter clearly plays an important role in diffusion within the global scale range when the first moment of the resting time distribution exists. The parameter  $\bar{\tau}$ , however, may not be applicable if the resting time distribution is of a power type with non-existing first moment  $\bar{\tau}$ . In this case, alternative measures could be used such as, e.g., the median value. Our findings highlight the fact that in order to compare the results of particle diffusion at large time scales, the information about the resting times is needed. Thus, the next step in studying particle diffusion processes at large scales should involve physical experiments that would provide information on particle coordinates at large diffusion times including the rest periods.

**Acknowledgments** The authors are grateful to the reviewers for thorough reviews, constructive comments and useful suggestions that have been gratefully incorporated in the final manuscript. Funding for this research was provided in part by the Institute of Geophysics of the Polish Academy of Sciences through the Project for Young Scientists No. 16/IGF PAN/2011/Mi “Dynamics and topography of riverbed forms: an analysis of experimental data and modelling of sediment transport in the light of Einstein’s theory”, by Ministry of Sciences and Higher Education within statutory activities No. 3841/E-41/S/2015, and by EPSRC, UK (EP/G056404/1) within the project “High-resolution numerical and experimental studies of turbulence-induced sediment erosion and near-bed transport.”

**Open Access** This article is distributed under the terms of the Creative Commons Attribution 4.0 International License (<http://creativecommons.org/licenses/by/4.0/>), which permits unrestricted use, distribution, and reproduction in any medium, provided you give appropriate credit to the original author(s) and the source, provide a link to the Creative Commons license, and indicate if changes were made.

## References

1. Ballio F, Campagnol J, Nikora V, Radice A (2013) Diffusive properties of bed load moving sediments at short time scales. In: Proceedings of 2013 IAHR world congress, Chengdu, China (CD)
2. Bialik RJ (2011) Particle-particle collision in Lagrangian modelling of saltating grains. *J Hydraul Res* 49(1):23–31. doi:[10.1080/00221686.2010.543778](https://doi.org/10.1080/00221686.2010.543778)
3. Bialik RJ, Nikora VI, Rowiński PM (2012) 3D Lagrangian modelling of saltating particles diffusion in turbulent water flow. *Acta Geophys* 60(6):1639–1660. doi:[10.2478/s11600-012-0003-2](https://doi.org/10.2478/s11600-012-0003-2)
4. Bialik RJ (2013) Numerical study of near-bed turbulence structures influence on the initiation of saltating grains movement. *J Hydrol Hydromech* 61(3):202–207. doi:[10.2478/johh-2013-0026](https://doi.org/10.2478/johh-2013-0026)

5. Bradley DN, Tucker GE, Benson DA (2010) Fractional dispersion in a sand bed river. *J Geophys Res* 115:F00A09. doi:[10.1029/2009JF001268](https://doi.org/10.1029/2009JF001268)
6. Drake TG, Shreve RL, Dietrich WE, Whiting PJ, Leopold LB (1988) Bedload transport of fine gravel observed by motion-picture photography. *J Fluid Mech* 192:193–217. doi:[10.1017/S0022112088001831](https://doi.org/10.1017/S0022112088001831)
7. Einstein HA (1937) *Der Geschiebebetrieb als Wahrscheinlichkeitsproblem*. Verlag Rascher, Zurich
8. Einstein HA (1950) The bed-load function for sediment transportation in open channel flows. Tech Bull 1026, US Department of Agriculture, Washington, DC
9. Feller W (1968) *An introduction to probability theory and its applications*, vol 1. Wiley, New York
10. Furbish DJ, Ball AE, Schmeeckle MW (2012) A probabilistic description of the bed load sediment flux: 4. Fickian diffusion at low transport rates. *J Geophys Res* 117:F03034. doi:[10.1029/2012JF002356](https://doi.org/10.1029/2012JF002356)
11. Habersack HM (2001) Radio-tracking gravel particles in a large braided river in New Zealand: a field test of the stochastic theory of bed load transport proposed by Einstein. *Hydrol Process* 15(3):377–391. doi:[10.1002/hyp.147](https://doi.org/10.1002/hyp.147)
12. Hassan MA, Church M, Schick AP (1991) Distance of movement of coarse particles in gravel bed streams. *Water Resour Res* 27(4):503–511. doi:[10.1029/90WR02762](https://doi.org/10.1029/90WR02762)
13. Hill KM, DellAngelo L, Meerschaert MM (2010) Heavy-tailed travel distance in gravel bed transport: an exploratory enquiry. *J Geophys Res* 115:F00A14. doi:[10.1029/2009JF001276](https://doi.org/10.1029/2009JF001276)
14. Martin RL, Jerolmack DJ, Schumer R (2012) The physical basis for anomalous diffusion in bed load transport. *J Geophys Res* 117:F01018. doi:[10.1029/2011JF002075](https://doi.org/10.1029/2011JF002075)
15. Martin RL, Purohit PK, Jerolmack DJ (2014) Sedimentary bed evolution as a mean-reverting random walk: implications for tracer statistics. *Geophys Res Lett* 41:6125–6159. doi:[10.1002/2014GL060525](https://doi.org/10.1002/2014GL060525)
16. Nikora V, Heald J, Goring D, McEwan I (2001) Diffusion of saltating particles unidirectional water flow over a rough granular bed. *J Phys A Math Gen* 34(50). doi:[10.1088/0305-4470/34/50/103](https://doi.org/10.1088/0305-4470/34/50/103)
17. Nikora V, Habersack H, Huber T, McEwan I (2002) On bed particle diffusion in gravel bed flows under weak bed load transport. *Water Resour Res* 38(6). doi:[10.1029/2001WR000513](https://doi.org/10.1029/2001WR000513)
18. Roseberry JC, Schmeeckle MW, Furbish DJ (2012) A probabilistic description of the bed load sediment flux: 2. Particle activity and motions. *J Geophys Res* 117:F03032. doi:[10.1029/2012JF002353](https://doi.org/10.1029/2012JF002353)
19. Sayre W, Hubbell D (1965) Transport and dispersion of labeled bed material, North Loup River, Nebraska. *US Geol Surv Prof Pap* 433(C):1–48
20. Voepel H, Schumer R, Hassan MA (2013) Sediment residence time distributions: theory and application from bed elevation measurements. *J Geophys Res* 118:2557–2567. doi:[10.1002/jgrf.20151](https://doi.org/10.1002/jgrf.20151)
21. Witz MJ (2014) *Mechanics of particle entrainment in turbulent open-channel flows*. PhD Thesis, University of Aberdeen, p 221
22. Zhang Y, Meerschaert MM, Packman AI (2012) Linking fluvial bed sediment transport across scales. *Geophys Res Lett* 39:L20404. doi:[10.1029/2012GL053476](https://doi.org/10.1029/2012GL053476)